



Caustic networks with customized intensity statistics

PHILIP MENZ,¹  ALESSANDRO ZANNOTTI,¹ CORNELIA DENZ,^{1,2}
AND JÖRG IMBROCK^{1,*} 

¹*Institute of Applied Physics, University of Muenster, 48149 Muenster, Germany*

²*Physikalisch-Technische Bundesanstalt (PTB), Bundesallee 100, 38116 Braunschweig, Germany*

*imbrock@uni-muenster.de

Abstract: Controlling random light is a key enabling technology that pioneered statistical imaging methods like speckle microscopy. Such low-intensity illumination is especially useful for bio-medical applications where photobleaching is crucial. Since the Rayleigh intensity statistics of speckles do not always meet the requirements of applications, considerable effort has been dedicated to tailoring their intensity statistics. A special random light distribution that naturally comes with radically different intensity structures to speckles are caustic networks. Their intensity statistics support low intensities while allowing sample illumination with rare rouge-wave-like intensity spikes. However, the control over such light structures is often very limited, resulting in patterns with inadequate ratios of bright and dark areas. Here, we show how to generate light fields with desired intensity statistics based on caustic networks. We develop an algorithm to calculate initial phase fronts for light fields so that they smoothly evolve into caustic networks with the desired intensity statistics during propagation. In an experimental demonstration, we exemplarily realize various networks with a constant, linearly decreasing and mono-exponential probability density function.

Published by Optica Publishing Group under the terms of the [Creative Commons Attribution 4.0 License](https://creativecommons.org/licenses/by/4.0/). Further distribution of this work must maintain attribution to the author(s) and the published article's title, journal citation, and DOI.

1. Introduction

Imaging with structured light enables new standards in resolution, accuracy or signal throughput. Examples cover STED microscopy with Gaussian vortex beams [1] as well as light sheet microscopy with Bessel- and Airy beams [2,3]. It is no coincidence that all these beam structures are determined by caustics [4] which define their high-intensity profiles as the envelope of rays [5].

Besides such regular beams, even random light structures like speckle patterns offer a certain degree of controllability alongside with beneficial intensity Rayleigh statistics and Fourier spectra [6–8] that enable imaging applications ranging from the smallest scales in speckle microscopy [9–11] to the largest scales in stellar speckle interferometry [12].

In the last years, the advantages of random light were further developed by customizing the speckle distribution and their intensity statistics towards non-Rayleigh speckles in 2D [13–17] and 3D [18,19], providing prospects in dynamic speckle illumination microscopy [9], super-Rayleigh photoacoustic imaging [10,11,20], super-resolution microscopy [21], and measuring atmospheric optical turbulences [22].

Speckles are closely related to caustic networks. Both emerge from phase fluctuations described as Gaussian random fields (GRFs) [12,15,23]. While speckles are the far-field pendant to GRFs, their near-field focusing leads to the ramified intensity networks like those formed by sunrays on the bottom of swimming pools. Recent works suggest to utilize the naturally given macroscopic and incoherent caustic networks in shallow sea for stereoscopic and single-pixel underwater vision [24–26] working over a range of wavelengths and length scales without the need for

detector arrays, and possibly with quantum light, where the correlations of entangled photons can be exploited. As well, artificial counterparts of caustic networks in laser light support single-exposure 3D imaging [27]. We emphasize the use of caustic networks with customized intensity statistics for imaging applications, including microscopy of photosensitive samples or advanced stereoscopic vision of large structures with a range of wavelengths.

Caustics are the envelopes of families of rays and characterized by an abrupt increase of the fields' wave function in their vicinity [5]. They appear not only in light as ray optics description, but more general as branched flows [28] for particles e.g. in semiconductors [29], currents that form tsunamis [30,31], or affect the formation of oceanographic [32] and optical rogue waves [33,34]. In wave optics, a wave that acquires random phase fluctuations with a correlation length larger than the wavelength develops a network of random caustics in the near field by linear free-space propagation [35].

The focusing of waves to caustic networks assumes initial Gaussian distributed phase fluctuations [15,35]. These phase fluctuations focus light to caustic networks with highly non-Gaussian intensity statistics in form of heavy-tailed distributions, thus containing high-intensity contributions which are optical rogue waves [33,34,36]. As the wave propagates far beyond the focal plane speckle patterns are formed in the far field, whose intensity obeys Rayleigh statistics [6,37,38]. The analogies between optics and oceanography, where within certain limits the wave dynamics in both systems is governed by the nonlinear Schrödinger equation, allow to exploit optics as a platform to study linear and non-linear mechanisms for the formation of rogue waves [34,39–41].

Inspired by previously presented works in which the intensity statistics of speckles were tailored [15,16], and by caustic-based beam design approaches [42], we turn the close relation between speckles and caustic networks to account and present a general method to customize the intensity statistics of caustic networks. This method can easily be adopted to transform any original light field to a new light field with desired probability density function (PDF) and at any plane. For this purpose, we perform a local intensity transformation of the generated caustic network towards an intensity network with a desired PDF. Knowing this target intensity, we numerically re-calculate a generating initial phase mask that focuses onto the aimed network during propagation. We realize experimentally caustic networks with novel intensity statistics and exemplarily demonstrate PDFs that follow a mono-exponential curve (which originally is a characteristics of speckles), are constantly distributed, or even linearly decaying. Finally, we demonstrate that these light fields form smoothly during propagation, which is often challenging as light fields focus abruptly using standard Gerchberg-Saxton algorithms [43]. We therefore show that their PDFs transform steadily during propagation and are customized in the desired target plane while showing speckle-like Rayleigh distributions far away from the target plane.

2. Algorithm and experimental system to generate customized caustic networks

When a plane wave experiences phase fluctuations in form of a two-dimensional Gaussian random field (GRF) $\phi(\mathbf{r}_\perp)$, the resulting light field $E = \exp[i\Delta\phi(\mathbf{r}_\perp)]$ focuses to a caustic network during propagation. Here $\phi(\mathbf{r}_\perp) \in [0, 2\pi)$ and $\Delta \in \mathbb{Z}$ is the phase amplitude. The initial GRF phase distribution varies smoothly and is characterized by a Gaussian spatial auto-correlation function. We generate the initial GRF phase distribution by multiplying a random, uniformly distributed seed $\kappa(\mathbf{r}_\perp)$ to the square root of a Gaussian spectral power density $\mathcal{F}[\exp(-r^2/2\ell_c^2)]$ with correlation length ℓ_c [23,31,44,45],

$$\phi(\mathbf{r}_\perp) = \mathcal{F}^{-1} \left[e^{-i\kappa(\mathbf{r}_\perp)} \sqrt{\mathcal{F} \left[e^{-\frac{r^2}{2\ell_c^2}} \right]} \right]. \quad (1)$$

The experimental system we use to realize and capture the custom caustic network light fields is shown in Fig. 1. We address Δ times the GRF as a phase mask to a spatial light modulator (SLM)

'Holoeye Heo' and illuminate it with a plane wave of wavelength $\lambda = 532$ nm. The phase-only SLM allows encoding amplitude and phase simultaneously by using a Fourier filter (FF) [46]. We image the light field addressed onto the SLM using a telescope consisting of two lenses, L_1 ($f = 385$ mm) and L_2 ($f = 38$ mm), with a de-magnification of 10.1 onto a plane which we refer to as the origin at $z = z_0 = 0$ mm. The propagating light field forms a caustic network at the target plane at $z = z_t = 1.98$ mm and is detected using an imaging system consisting of a microscope objective (MO) Olympus MPLN with a magnification of 10 and numerical aperture of 0.25 and a camera iDS UI-3370CP-M-GL. In order to record the propagation of a light field, both imaging objects are mounted on a linear stage that is movable in z -direction, imaging alternately the planes $z = 0$ and $z = z_t$ and also further distances up to $z = 10z_t$ [42]. We determine the sharpest plane of the caustic network as where its contrast reaches 1 due to the formation of zeros of intensity (optical vortices) in the light field. To recover the spatial phase structure of our light fields, we employ a standard digital holographic method based on the superposition of the signal wave with a tilted reference wave [47]. This second beam can be switched off using a shutter (S).

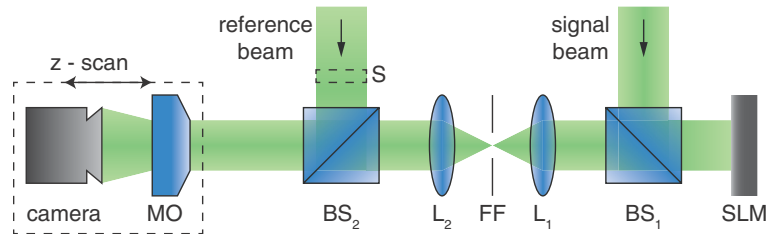


Fig. 1. Experimental setup. Cw laser source at $\lambda = 532$ nm generating a signal and a reference beam, respectively. SLM: spatial light modulator, BS: beam splitter, L_1 : lens with $f = 385$ mm, L_2 : lens with $f = 38$ mm, FF: Fourier filter, MO: microscope objective Olympus MPLN, S: shutter, camera iDS UI-3370CP-M-GL.

We control the distance to the focal plane and the sharpness of the caustics by the correlation length ℓ_c and phase amplitude Δ . Throughout this work, we choose $\ell_c = 38$ μm and $\Delta = 2$ to meet the dimensions of our experimental system in terms of resolution and recordable propagation distance. These parameters crucially affect the network's probability density function (PDF) in the target plane [23,35,45]. The heavy-tailed PDFs $P(I)$ of caustic networks are characterized by stretched exponential functions $A \exp[-B(I/\langle I \rangle)^C]$, where A, B, C are fit parameters and $\langle I \rangle$ denotes the transverse mean intensity. Decreasing values of $C < 1$ indicate an increasing number of rogue events [33,35,48,49]. In contrast, speckle patterns show a mono-exponential decay with $C = 1$ [6–8].

Subsequently, taking the original intensity statistics $P(I)$ as a basis, we determine a local intensity transformation $\tilde{I} = f(I)$ to transform the original caustic network into a network with customized intensity PDF $F(\tilde{I})$ [15,16]. The transformation function $f(I)$ is calculated by relating the PDF $P(I)$ of a caustic network to the targeted customized intensity PDF $F(\tilde{I})$

$$\int_0^I P(I') dI' = \int_0^{\tilde{I}} F(\tilde{I}') d\tilde{I}'. \quad (2)$$

For a given caustic network obtained at z_t , we integrate the left hand side of (2) numerically and solve for \tilde{I} as a function of I . Thereby, the desired intensity PDF $F(\tilde{I})$ needs to obey the normalization conditions $\int_0^{\tilde{I}_{\max}} F(\tilde{I}') d\tilde{I}' = 1$ and $\langle \tilde{I} \rangle = \int_0^{\tilde{I}_{\max}} \tilde{I}' F(\tilde{I}') d\tilde{I}' = \langle I \rangle$ [15,16]. Without loss of generality, we choose $\langle I \rangle = 1$. Note that, unlike in [15], we do not fit the left hand side of (2) with a function, instead we integrate each caustic network completely numerically. Contrary to speckles, caustic networks do not have a monoexponentially decaying PDF but a

stretched one. Even keeping the l_c and Δ parameters unchanged, the stretch parameter C can vary. Therefore, a numerical integration gives much better accuracy with a minor time consumption tradeoff. Having calculated the intensity transformation $f(I)$ and having applied it to the caustic network, we yield the target intensity distribution in the focal plane z_t . A challenging task is now to determine an initial phase distribution of the light field at z_0 that focuses to this particular intensity distribution as its target. Therefore, we calculate an initial phase distribution via a modified Gerchberg-Saxton algorithm [43], schematically presented in Fig. 2.

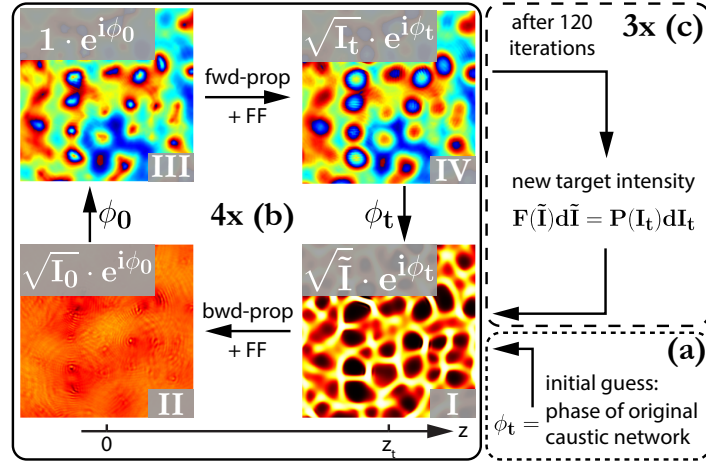


Fig. 2. Schematic illustration of the modified Gerchberg-Saxton algorithm for the phase retrieval of caustic networks with customized intensity PDFs. The initial input (a) is passed to the main block (b), which is then iterated 120 times. This intermediate result is passed to block (c), where a new target intensity is calculated. This outer loop is executed 3 times.

The algorithm starts by synthesizing a light field $\psi(\mathbf{r}_\perp, z_t) = \sqrt{\tilde{I}} \exp(i\phi_t)$ assembled by the square root of the calculated target intensity \tilde{I} as an amplitude and the phase of the original caustic network ϕ_t in the focal plane at z_t , see Fig. 2(I) where this target intensity is pictured. We emphasize that this phase is not the GRF, which would be present at the first iteration step at z_0 . The resulting light field $\psi(\mathbf{r}_\perp, z_t)$ propagates backwards to the origin at z_0 using a paraxial spectral Fresnel propagator [50]

$$\psi(\mathbf{r}_\perp, 0) = \mathcal{F}^{-1} \left\{ \exp \left[iL_z(k_x^2 + k_y^2)/(2k) \right] \mathcal{F} [\psi(\mathbf{r}_\perp, z + L_z)] \right\}. \quad (3)$$

Before performing the inverse Fourier transforms in (3), we low-pass filter the light field (FF) by a Gaussian window function with a size comparable to the real physical dimensions of approximately $600 \times 600 \mu\text{m}$ corresponding to the field of view in our experiment. Note that no filtering leads to unphysical, abruptly forming intensity distributions showing exactly the desired PDF in the simulations but may never be realized experimentally due to unrealistic high Fourier frequencies.

Taking the light field at z_0 , we extract its phase ϕ_0 , depicted in Fig. 2(III), which serves as a new guess for an initial light field, while we replace the current intensity I_0 , shown exemplary after a few iterations in Fig. 2(II), with a spatially homogeneous one. The resulting light field propagates forward to the target plane at z_t . During this propagation, we once again low-pass filter the light field in Fourier space (FF). In the target plane, the calculated phase, shown in Fig. 2(IV), remains and the amplitude is again replaced by the square root of the target intensity, see Fig. 2(IV->I). This algorithm is iterated several times until the resulting intensity distribution

does not change significantly anymore. We found this to be the case after 120 iterations since no notable improvement was achieved after that point.

However, due to the physical limitations of finite apertures in the experimental system, here mimicked by the Fourier filtering, the PDF has not fully adopted the desired shape. Based on this intermediate result, we recalculate a new target intensity according to Eq. (2) and repeat the Gerchberg-Saxton process. Essentially, we repeat the first procedure of calculating an intensity transformation, but instead of the original caustic network, we recalculate a target intensity from the intensity output of the Gerchberg-Saxton algorithm. Together with this second nested procedure, the algorithm is repeated a few times until no significant improvement of the desired intensity PDF is achieved. In our case, we iterate the main block of the algorithm, see Fig. 2(b), 4 times and perform the recalculation 3 times, see Fig. 2(c). Eventually, we are able to calculate an initial phase mask that focuses to a caustic network with customized intensity statistics with very good agreement to the desired PDF. As a result, we obtain a new initial phase pattern $\phi_2(\mathbf{r}_\perp)$ that interestingly differs only slightly from the original pattern.

The representation of the desired intensity statistics in the realized light field depends on the size of the field of view, or respectively on the number of realizations. By choosing the field of view properly and averaging over many realizations, we can rule out edge effects and evaluate the pure method. Therefore, for each PDF to be realized, we generate a large number of 99 different light fields, calculate the individual intensity statistics and average over all of them.

3. Realization of caustic networks with customized intensity statistics

Examples of experimental results that we obtain using our approach are shown in Fig. 3. Figure 3(a) shows an original (unmodified) phase mask of $\Delta \cdot \text{GRF}$ at z_0 that gives rise to the caustic network depicted in Fig. 3(b) recorded in the target plane at z_t . Note that all presented caustic networks are individually normalized to $\langle I \rangle = 1$ and scaled to their respective maximum. While the transverse patterns presented in Fig. 3 exemplary show one case of 99 randomly generated caustic networks, all 99 contribute to the presented histograms. That is, averaging over the histograms of all caustic networks yields the histogram shown in Fig. 3(c). The histogram shows the probability density $P(I/\langle I \rangle)$ that a certain normalized intensity $I/\langle I \rangle$ occurs. As expected for the case of a **standard caustic network** shown in Figs. 3(a)–3(c), we observe a heavy-tailed PDF with rogue wave characteristics [33,35]. Such PDFs are often described by stretched exponential functions which obey $P(I/\langle I \rangle) = A \exp[-B(I/\langle I \rangle)^C]$ [33,35,49,51]. Using a stretched exponential fit function, we obtain $C = 0.415 \pm 0.026$. The curve is shown in Fig. 3(c) as a red dashed line. It indicates rogue wave formation, far away from speckle characteristics with $C = 1$. Note the semi-log plot for the histograms Figs. 3(c) and 3(f), while the histograms in Figs. 3(i) and 3(l) have a linear scale. Figs. 3(d)–3(f) shows the case of a caustic network with a (non-stretched) **mono-exponential** PDF, i.e. $C = 1$, typical for Rayleigh speckle patterns [6]. Figure 3(d) shows the phase mask which we calculate using the presented algorithm and which we address to the SLM at z_0 . In the target plane at z_t the modified caustic network forms, shown in Fig. 3(e). Its histogram presented in Fig. 3(f) follows a mono-exponential function $F(\tilde{I}/\langle \tilde{I} \rangle) = \exp(-\tilde{I}/\langle \tilde{I} \rangle)$. This desired curve is indicated as red dashed line. A corresponding line fit yields a goodness of the fit, described by the coefficient of determination, of $R^2 = 0.992$, thus confirms that the histogram is largely non-stretched. Interestingly, these Rayleigh intensity statistics belong to those of speckle patterns [6,7,12,15] but in our modified case show pronounced and filigree intensity networks that surround many dark areas. This result holds attractive potentials. It shows that all speckle-based applications could benefit from customized light fields which still have Rayleigh statistics but a different appearance of their intensity distributions. As so, dynamically changing patterns may serve as illuminating light for microscopy of photo-sensitive samples or for super-resolution imaging [9–11,21].

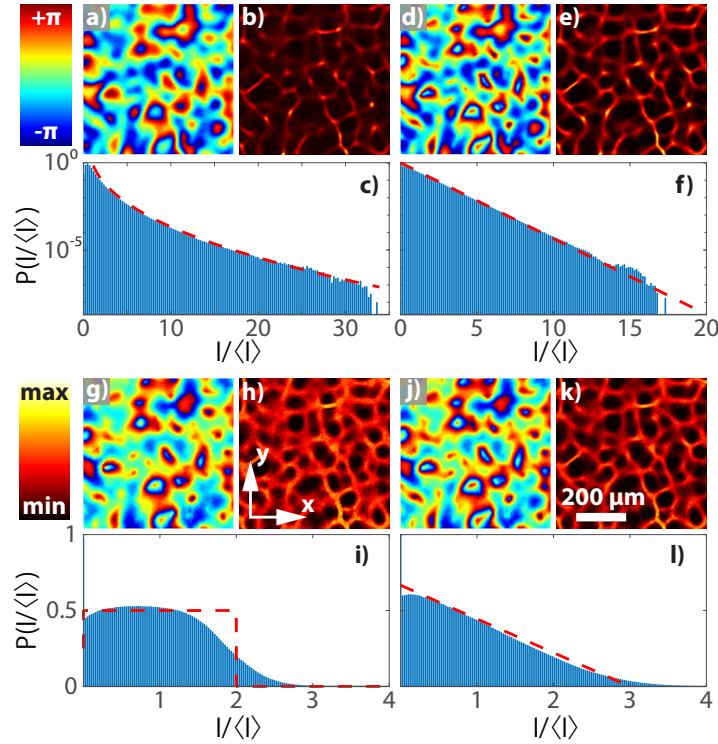


Fig. 3. Examples of caustic networks with modified intensity PDFs. The developed algorithm generates the initial phases (a, d, g, j), which focus to the respective intensity distributions (b, e, h, k) in the target plane. Averaged over 99 independent caustic networks, we calculate the intensity histograms (c, f, i, l). The blue bars are experimental data, while the dashed red curves indicate the desired PDFs for the three customized cases (f, i, l) and represents a stretched exponential fit in image (c). Note the semi-log scale in (c, f) and the linear scale in (i, l).

As an extreme example, where the original PDF of Fig. 3(c) is drastically altered, we demonstrate the realized caustic network and its PDF when aiming for a **constant** PDF in Figs. 3(g)–3(i). The generating phase mask in Fig. 3(g) focuses to the caustic network intensity of Fig. 3(h). The desired PDF obeys the constant value $F(\tilde{I}/\langle\tilde{I}\rangle) = 0.5$ over a range from $0 < \tilde{I}/\langle\tilde{I}\rangle < 2$ and is shown by the red dashed curve. The experimentally obtained histogram exhibits a broad plateau in its center where it is nearly constant and violates this target at the borders for the minimal and maximal values of $\tilde{I}/\langle\tilde{I}\rangle$. As sharp edges in the histogram are physically not realizable, this case is particularly challenging. Fitting the measured histogram with the desired PDF, we yield $R^2 = 0.873$. Sharper edges of the histogram may be obtained when higher Fourier frequencies contribute to the light field, thus using larger apertures in the experiment.

Furthermore, we demonstrate intensity networks with a **linearly decaying** target PDF $F(\tilde{I}/\langle\tilde{I}\rangle) = 2/9(3 - \tilde{I}/\langle\tilde{I}\rangle)$ for $0 < \tilde{I}/\langle\tilde{I}\rangle < 3$ (Figs. 3(j)–3(l)). This curve is shown in Fig. 3(l) as a red dashed line. The concrete slope of this curve is a consequence of the normalization conditions for the PDFs described in Sec. 2. Though deviations are apparent especially for low normalized intensities, in general the linear slope of the customized histogram is well realized. Fitting the experimentally obtained histogram with the expected PDF yields a goodness of $R^2 = 0.988$.

4. Evolution of a customized caustic network

Gerchberg-Saxton and related algorithms often have the limitation that the desired transverse intensity distributions abruptly form in the target plane, and thus react sensitively on the longitudinal distance [52]. Such spontaneously changing patterns require high Fourier components and are often not experimentally realizable. Since the presented approach accounts for finite apertures in the experimental system by filtering the field in Fourier space (FF), see Sec. 2, only Fourier components that are supported by the experimental system contribute to the field. As a consequence, the evolution of the intensity pattern during propagation occurs smoothly. In this section we show that the customized caustic networks with desired PDFs evolve to speckle patterns when propagating beyond the target plane from z_t to distances up to $10z_t$. These distances from 1.98 mm – 19.8 mm span the regime between the Fresnel region ($F \approx 1$) and the far field, as the Fresnel number of the furthest plane $F = \ell_c^2 / (10z_t \lambda) \approx 0.14$ begins to fulfill the Fraunhofer diffraction condition $F \ll 1$ [53]. A similar effect was already described in previous works but for modified speckle patterns in the far field [15,17].

Figure 4 shows the experimentally obtained intensity and the phase distributions of a caustic network with a customized PDF, exemplary for the case of a mono-exponential PDF (Figs. 3(d)–3(f)) at different propagation distances $z = 1.98$ mm, 3.96 mm, 5.94 mm, 19.80 mm. For each propagation distance, we show the experimentally measured PDFs, averaged over 99 realizations.

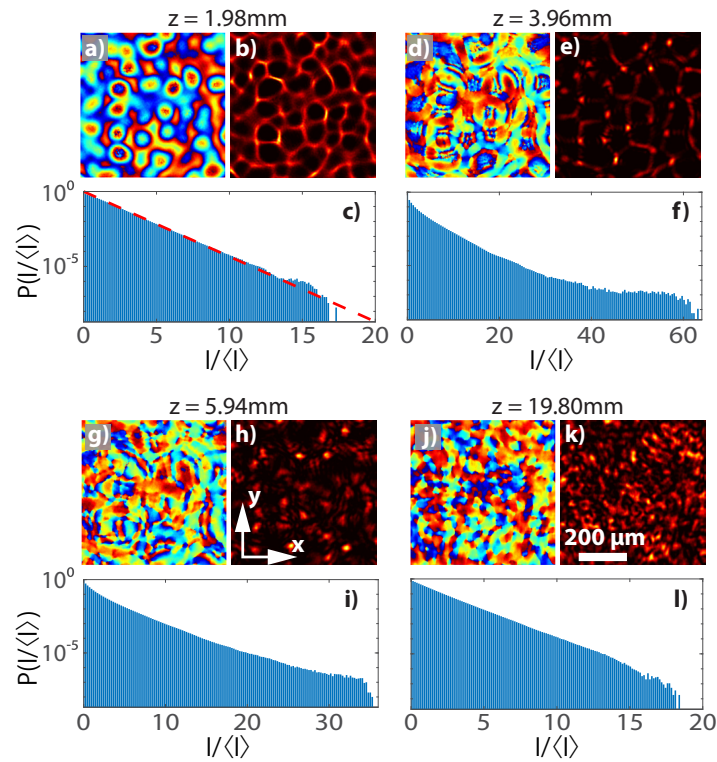


Fig. 4. Transverse phase (a), transverse intensity (b), and intensity PDF (c) (averaged over 99 independent caustic networks) of the mono-exponential case at a propagation distance of $z = 1z_t$. (d-f) Same as (a-c), but at $z = 2z_t$. (g-i) Same as (a-c), but at $z = 3z_t$. (j-l) Same as (a-c), but at $z = 10z_t$. With $z_t = 1.98$ mm. All PDFs shown with semi-log scale.

The results shown in Fig. 4 comprise a two-fold effect. On the one hand, the PDFs show that the customized intensity statistics are only apparent in the focal plane z_t and blur during

propagation. The tailored Rayleigh statistics at z_t evolve via intermediate PDF states at $2z_t$ and $3z_t$. As the caustic networks have been calculated to exhibit the desired intensity statistics only in the target plane, like normal caustic networks, they evolve to speckles away from there, therefore in the intermediate regime the PDFs show a stretched exponential decay as to be expected from usual caustic networks. Propagating further to $10z_t$, the light field (partially) develops speckles, where the statistics converge to the corresponding Rayleigh distribution, representing a kind of intensity statistics recurrence. On the other hand, this particular example is outstanding since the desired PDF in the target plane z_t already follows the same statistics as speckles do, however showing sharp ramified intensity networks instead of granular isolated intensity spots of speckles.

5. Conclusions

We realize caustic networks with customized intensity statistics, showing exemplary intensity statistics that follow a mono-exponential decay, are constant, or are linearly decaying. Therefore, we develop an algorithm that calculates the initial pure phase modulation for light fields that propagate smoothly and form steadily customized caustic networks in the target plane. Propagating far away from the target plane, the caustic networks develop to speckle patterns.

Caustic networks with customized PDFs are particularly attractive for several applications that base on speckle illumination, though the appearance of the customized caustic networks shows a drastically different ratio of dark and bright areas. The demonstrated possibility to tune this ratio could improve current caustic network-based approaches like single-pixel and single-exposure imaging [26,27]. Customized caustic networks may also serve as counterparts to speckles in applications like optical micromanipulation tasks such as grinding, sieving and sorting [54]. They also hold promise as disordered potentials for colloidal particles and cold atoms, and in target applications where their optimized ramified intensity networks may prove beneficial over the isolated intensity spots of speckle patterns. The whole class of customized networks may have significance for imaging techniques, ranging over scales from micro- to macro-structures, and working with a broad range of wavelengths as well as incoherent light sources [24].

Funding. Westfälische Wilhelms-Universität Münster.

Acknowledgments. We acknowledge support from the Open Access Publication Fund of the University of Muenster.

Disclosures. The authors declare no conflicts of interest.

Data Availability. Data underlying the results presented in this paper are not publicly available at this time but may be obtained from the authors upon reasonable request.

References

1. S. W. Hell and J. Wichmann, "Breaking the diffraction resolution limit by stimulated emission: stimulated-emission-depletion fluorescence microscopy," *Opt. Lett.* **19**(11), 780–782 (1994).
2. F. O. Fahrbach, P. Simon, and A. Rohrbach, "Microscopy with self-reconstructing beams," *Nat. Photonics* **4**(11), 780–785 (2010).
3. T. Vettenburg, H. I. C. Dalgarno, J. Nylk, C. Coll-Lladó, D. E. K. Ferrier, T. Čížmár, F. J. Gunn-Moore, and K. Dholakia, "Light-sheet microscopy using an Airy beam," *Nat. Methods* **11**(5), 541–544 (2014).
4. M. A. Alonso and M. R. Dennis, "Ray-optical Poincaré sphere for structured Gaussian beams," *Optica* **4**(4), 476–486 (2017).
5. M. V. Berry and C. Upstill, "Catastrophe optics: Morphologies of caustics and their diffraction patterns," *Prog. Opt.* **18**, 257–346 (1980).
6. J. W. Goodman, "Some fundamental properties of speckle," *J. Opt. Soc. Am.* **66**(11), 1145–1150 (1976).
7. P. Jacquot and J.-M. Fournier, *Interferometry in Speckle Light* (Springer-Verlag, Berlin, Heidelberg, 2000).
8. L. C. Andrews and R. L. Phillips, *Laser Beam Propagation through Random Media* (SPIE Press, Bellingham, Washington, USA, 2005), 2nd ed.
9. C. Ventalon and J. Mertz, "Dynamic speckle illumination microscopy with translated versus randomized speckle patterns," *Opt. Express* **14**(16), 7198–7209 (2006).
10. J. Gateau, T. Chaigne, O. Katz, S. Gigan, and E. Bossy, "Improving visibility in photoacoustic imaging using dynamic speckle illumination," *Opt. Lett.* **38**(23), 5188–5191 (2013).

11. T. Chaigne, J. Gateau, M. Allain, O. Katz, S. Gigan, A. Sentenac, and E. Bossy, "Super-resolution photoacoustic fluctuation imaging with multiple speckle illumination," *Optica* **3**(1), 54–57 (2016).
12. J. C. Dainty, *Laser Speckle and Related Phenomena* (Springer, Berlin, Heidelberg, 1975).
13. Y. Bromberg and H. Cao, "Generating non-Rayleigh speckles with tailored intensity statistics," *Phys. Rev. Lett.* **112**(21), 213904 (2014).
14. X. Li, Y. Tai, H. Li, J. Wang, H. Wang, and Z. Nie, "Generation of a super-Rayleigh speckle field via a spatial light modulator," *Appl. Phys. B* **122**(4), 82 (2016).
15. N. Bender, H. Yilmaz, Y. Bromberg, and H. Cao, "Customizing Speckle Intensity Statistics," *Optica* **5**(5), 595–600 (2018).
16. N. Bender, H. Yilmaz, Y. Bromberg, and H. Cao, "Creating and controlling complex light," *APL Photonics* **4**(11), 110806 (2019).
17. N. Bender, H. Yilmaz, Y. Bromberg, and H. Cao, "Introducing non-local correlations into laser speckles," *Opt. Express* **27**(5), 6057–6067 (2019).
18. R. Liu, B. Qing, S. Zhao, P. Zhang, H. Gao, S. Chen, and F. Li, "Generation of non-rayleigh nondiffracting speckles," *Phys. Rev. Lett.* **127**(18), 180601 (2021).
19. S. Han, N. Bender, and H. Cao, "Tailoring 3d speckle statistics," *Phys. Rev. Lett.* **130**(9), 093802 (2023).
20. P. Liu, "Label-free STORM principle realized by super-Rayleigh speckle in photoacoustic imaging," *Opt. Lett.* **44**(19), 4642–4645 (2019).
21. N. Bender, M. Sun, H. Yilmaz, J. Bewersdorf, and H. Cao, "Circumventing the optical diffraction limit with customized speckles," *Optica* **8**(2), 122–129 (2021).
22. H. Mei, H. Ye, L. Kang, X. Qian, H. Huang, Y. Huang, W. Zhu, X. Wu, and R. Rao, "Principle and feasibility of using a 3M reflective film based fold pass laser speckle imaging system for measuring atmospheric optical turbulence," *OSA Continuum* **2**(6), 1938–1952 (2019).
23. J. J. Metzger, "Branched Flow and Caustics in Two-Dimensional Random Potentials and Magnetic Fields," Dissertation, Georg-August-Universität zu Göttingen (2010).
24. Y. Swirski, Y. Y. Schechner, B. Herzberg, and S. Negahdaripour, "CauStereo: Range from light in nature," *Appl. Opt.* **50**(28), F89–F101 (2011).
25. M. Zhao, J. Uhlmann, M. Lanzagorta, J. Kanugo, A. Parashar, O. Jitrik, and S. E. Venegas-Andraca, "Passive ghost imaging using caustics modeling," *Proc. SPIE* **10188**, 101880H (2017).
26. E. Toninelli, D. Stellinga, B. Sephton, A. Forbes, and M. J. Padgett, "Single-pixel imaging using caustic patterns," *Sci. Rep.* **10**(1), 2281 (2020).
27. N. Antipa, G. Kuo, R. Heckel, B. Mildenhall, E. Bostan, R. Ng, and L. Waller, "DiffuserCam: lensless single-exposure 3D imaging," *Optica* **5**(1), 1–9 (2018).
28. T. Poston and I. Stewart, *Catastrophe Theory and its Applications* (Dover Publications, Inc., Mineola, New York, 1996), 1st ed.
29. M. A. Topinka, B. J. LeRoy, R. M. Westervelt, S. E. Shaw, R. Fleischmann, E. J. Heller, K. D. Maranowski, and A. C. Gossard, "Coherent branched flow in a two-dimensional electron gas," *Nature* **410**(6825), 183–186 (2001).
30. M. V. Berry, "Focused tsunami waves," *Proc. R. Soc. A* **463**(2087), 3055–3071 (2007).
31. H. Degueldre, J. J. Metzger, T. Geisel, and R. Fleischmann, "Random focusing of tsunami waves," *Nat. Phys.* **12**(3), 259–262 (2016).
32. C. Kharif and E. Pelinovsky, "Physical mechanisms of the rogue wave phenomenon," *European Journal of Mechanics, B/Fluids* **22**(6), 603–634 (2003).
33. A. Mathis, L. Froehly, S. Toenger, F. Dias, G. Genty, and J. M. Dudley, "Caustics and rogue waves in an optical sea," *Sci. Rep.* **5**(1), 12822 (2015).
34. N. Akhmediev, B. Kibler, and F. Baronio, *et al.*, "Roadmap on optical rogue waves and extreme events," *J. Opt.* **18**(6), 063001 (2016).
35. A. Safari, R. Fickler, M. J. Padgett, and R. W. Boyd, "Generation of Caustics and Rogue Waves from Nonlinear Instability," *Phys. Rev. Lett.* **119**(20), 203901 (2017).
36. M. Mattheakis, I. J. Pitsios, G. P. Tsironis, and S. Tzortzakakis, "Extreme events in complex linear and nonlinear photonic media," *Chaos, Solitons Fractals* **84**, 73–80 (2016).
37. J. W. Goodman, *Introduction to Fourier optics* (Roberts & Company Publishers, Greenwood Village, 2005), 3rd ed.
38. O. V. Angelsky, P. P. Maksimyak, A. P. Maksimyak, and Y. A. Ushenko, "The role of caustics in formation of network of amplitude zeroes in speckle field," *Appl. Opt.* **43**(31), 5744–5753 (2004).
39. N. Akhmediev, J. M. Dudley, D. R. Solli, and S. K. Turitsyn, "Recent progress in investigating optical rogue waves," *J. Opt.* **15**(6), 060201 (2013).
40. J. M. Dudley, F. Dias, M. Erkintalo, and G. Genty, "Instabilities, breathers and rogue waves in optics," *Nat. Photonics* **8**(10), 755–764 (2014).
41. J. M. Dudley, G. Genty, A. Mussot, A. Chabchoub, and F. Dias, "Rogue waves and analogies in optics and oceanography," *Nat. Rev. Phys.* **1**(11), 675–689 (2019).
42. A. Zannotti, C. Denz, M. A. Alonso, and M. R. Dennis, "Shaping caustics into propagation-invariant light," *Nat. Commun.* **11**(1), 3597 (2020).
43. R. W. Gerchberg and W. O. Saxton, "Practical Algorithm for the Determination of Phase From Image and Diffraction Plane Pictures," *Optik (Stuttgart)* **35**(2), 237–246 (1972).

44. S. Barkhofen, J. J. Metzger, R. Fleischmann, U. Kuhl, and H. J. Stöckmann, "Experimental observation of a fundamental length scale of waves in random media," *Phys. Rev. Lett.* **111**(18), 183902 (2013).
45. H. Degueldre, J. J. Metzger, E. Schultheis, and R. Fleischmann, "Channeling of Branched Flow in Weakly Scattering Anisotropic Media," *Phys. Rev. Lett.* **118**(2), 024301 (2017).
46. J. A. Davis, D. M. Cottrell, J. Campos, M. J. Yzuel, and I. Moreno, "Encoding amplitude information onto phase-only filters," *Appl. Opt.* **38**(23), 5004–5013 (1999).
47. T. Kreis, "Digital holographic interference-phase measurement using the Fourier-transform method," *J. Opt. Soc. Am. A* **3**(6), 847–855 (1986).
48. J. M. Dudley, M. Erkintalo, and G. Genty, "Rogue Waves of Light," *Opt. Photonics News* **26**(11), 34–41 (2015).
49. D. Pierangeli, F. Di Mei, C. Conti, A. J. Agranat, and E. DelRe, "Spatial Rogue Waves in Photorefractive Ferroelectrics," *Phys. Rev. Lett.* **115**(9), 093901 (2015).
50. G. Agrawal, *Nonlinear Fiber Optics* (Academic Press, 2013), 5th ed.
51. N. Marsal, V. Caultet, D. Wolfersberger, and M. Sciamanna, "Spatial rogue waves in a photorefractive pattern-forming system," *Opt. Lett.* **39**(12), 3690–3693 (2014).
52. C. Zhang, Y. Hu, W. Du, P. Wu, S. Rao, Z. Cai, Z. Lao, B. Xu, J. Ni, J. Li, G. Zhao, D. Wu, J. Chu, and K. Sugioka, "Optimized holographic femtosecond laser patterning method towards rapid integration of high-quality functional devices in microchannels," *Sci. Rep.* **6**(1), 33281 (2016).
53. M. Born and E. Wolf, *Principles of Optics* (Pergamon Press, Oxford, London, Edinburgh, New York, Toronto, Sydney, Paris, Braunschweig, 1970), 4th ed.
54. R. Jamali, F. Nazari, A. Ghaffari, S. K. Velu, and A.-R. Moradi, "Speckle tweezers for manipulation of high and low refractive index micro-particles and nano-particle loaded vesicles," *Nanophotonics* **10**(11), 2915–2928 (2021).